Measurement of Complex Optical Susceptibility for Individual Carbon Nanotubes by Elliptically Polarized Light Excitation

Fengrui Yao[1#], Can Liu[1#], Cheng Chen[1#], Shuchen Zhang[2], Qiuchen Zhao[2], Fajun Xiao[3], Muhong Wu[1], Jiaming Li[1], Peng Gao[4], Jianlin Zhao[3], Xuedong Bai[5], Shigeo Maruyama[6,7], Dapeng Yu[8], Enge Wang[4], Zhipei Sun[9,10], Jin Zhang[2], Feng Wang[11] and Kaihui Liu[1*]

[1] State Key Laboratory for Mesoscopic Physics, Collaborative Innovation Centre of Quantum Matter, School of Physics, Peking University, Beijing 100871, China

[2] Center for Nanochemistry, College of Chemistry and Molecular Engineering, Peking University, Beijing 100871, China

[3] School of Science, Northwestern Polytechnical University, Xi'an 710129, China

[4] International Center for Quantum Materials, Peking University, Beijing 100871, China

[5] Institute of Physics, Chinese Academy of Sciences, Beijing 100875, China

[6] Department of Mechanical Engineering, The University of Tokyo, Tokyo 113-8656, Japan

[7] Energy NanoEngineering Lab, National Institute of Advanced Industrial Science and Technology, Tsukuba 305-8564, Japan

[8] Department of Physics, Southern University of Science and Technology, Shenzhen 518055, China

[9] Department of Electronics and Nanoengineering, Aalto University, Espoo 02150, Finland

[10] QTF Centre of Excellence, Department of Applied Physics, Aalto University, Finland

[11] Department of Physics, University of California at Berkeley, Berkeley, California 94720, USA

#Theses authors contributed equally to this work

*Correspondence: khliu@pku.edu.cn

The complex optical susceptibility is the most fundamental parameter characterizing light-matter interactions and determining optical applications in any material. This parameter in three-dimensional bulk materials or two-dimensional films can be measured from the solution of Fresnel equations by conventional refraction or reflection measurements. However, in one-dimensional (1D) materials, as there is no concept of coherent refraction or reflection (Fresnel equations no longer apply), all conventional techniques to measure the complex susceptibility become invalid. Here we report a methodology to measure the complex optical susceptibility of individual 1D materials for the first time by an elliptical-polarization-based optical homodyne detection. This method is based on the accurate manipulation of interference between incident left- (right-) handed elliptically polarized light and the scattering light, which results in the opposite (same) contribution of the real and imaginary susceptibility in two sets of spectra and thus enables quantitative determination of complex susceptibility. We successfully demonstrate its application in determining complex susceptibility of individual chirality-defined carbon nanotubes in a broad optical spectral range (1.6-2.7 eV) and under different environments (suspended and in device). This full characterization of the complex optical responses should accelerate applications of various 1D nanomaterials (such as nanowires, nanorods, nanoribbons) in future photonic, optoelectronic, photovoltaic and bio-imaging devices.

One-dimensional (1D) materials are at the center of significant research effort of nano science and technology. For example, carbon nanotubes, a 1D material from rolled-up graphene, have shown fascinating optical properties, e.g. quantized optical transitions[1-3], strong many-body interactions[4-9] and efficient photon-electron generation[10], thus enabling diverse applications ranging from photonics[11-14], optoelectronics[15-17], photovoltaics[18] to bio-imaging[19]. To fully utilize 1D materials for various application, we need to know their optical response parameters that quantitatively describe light-matter interactions, among which the complex optical susceptibility ($\tilde{\chi}$) is the most fundamental one[20, 21] (describing the response of the dipole moment $\boldsymbol{P}$ of crystalline materials to external optical field $\boldsymbol{E}$, $\boldsymbol{P} = \tilde{\chi}\varepsilon_0\boldsymbol{E}$, $\tilde{\chi} = \tilde{\varepsilon} - 1$). Unlike mature technology for measuring the complex optical susceptibility by solving Fresnel equations in two-dimensional (2D) and three-dimensional (3D) materials[22], there is no available technique to effectively measure both the real and imaginary parts of $\tilde{\chi}$ in individual 1D materials. The main difficulty lies in the vanishing of concept for coherent refraction or reflection and thus conventional methodologies become invalid[23]. One way to circumvent this difficulty is to measure the absorption of 1D materials (e.g., carbon nanotubes[24-26]), which is proportional to the imaginary part susceptibility (χ_2). By employing the Kramers–Kronig (K-K) relation, one can in principle calculate the real part susceptibility χ_1. However, to get the accurate value, the application of K-K relation requires experimental data of χ_2 over an extremely broad energy region from 0 eV to infinity, which is never available. Till now, there is no method to directly measure the complex optical susceptibility of individual 1D materials.

Here we develop a new methodology to measure the complex optical susceptibility for individual carbon nanotubes by an elliptical-polarization-based optical homodyne detection. By accurately controlling the interference between incident left- and right-handed elliptical

polarization beam and nanotube scattering light, we obtain two sets of optical spectra containing both χ_1 and χ_2 information with different pre-coefficients, which allow us to determine the quantitative value of $\tilde{\chi}$. In addition, our technique also enhances the optical signal level by about two orders of magnitude, making the extremely weak individual nanotube signal readily detectable in a broad optical spectral range (1.6-2.7 eV) and under different environments (suspended and in device). Our results can open up exciting opportunities in characterizing a variety of 1D nanomaterials including graphene nanoribbon, nanowires, and other nano-biomaterials, thus facilitating their accurate material design and applications in future photonic, optoelectronic, photovoltaic, and bio-imaging devices.

Results

Scheme of complex optical susceptibility measurement in a transmission geometry.

For individual nanotubes with diameter (~1 nm) much less than light wavelength (~ 500 nm), their optical signal in reflection/transmission geometry can be viewed as the interference between optical reference and nanotube-scattering fields[27, 28]. To obtain both χ_1 and χ_2 of a nanotube, in principle we need two optical reference components with a $\pi/2$ phase difference. Actually, circularly/elliptically-polarized light naturally provides such a $\pi/2$ phase difference, which has been proved to be an effective excitation for optical tomography[29], spin/quantum computing and information[30], valleytronics[31] and high harmonic generation[32]. In our work, we choose elliptical polarization light with a relatively large ellipticity as excitation. Its advantage over circularly polarized light lies in that the reference beam can be greatly reduced by two vertically-placed polarizers, which will greatly enhance the final optical contrast as demonstrated in the previous single-tube Rayleigh scattering, absorption and reflection measurement using linear polarization excitation light[26, 33, 34].

We first apply this technique to individual suspended single-walled carbon nanotubes in a transmission geometry. Experimental scheme of our elliptical-polarization-based optical homodyne detection method is shown in Fig. 1a. A supercontinuum laser was used as the light source to provide a broadband excitation (450-800 nm), a pair of confocal polarization-maintaining objectives served to focus the supercontinuum light on individual nanotubes and collected the transmitting and nanotube-scattering lights, two polarizers and a quarter-wave plate were used to generate elliptically polarized light and control the polarization of transmitted light. Here we should note that the very careful selection of objectives and wave plate to maintain the polarization purity is crucial to realize the final signal detection (See optical component details in Methods). Layouts of the polarization control are shown in Fig. 1b and 1c. The two polarizers were set strictly perpendicular to each other, and the suspended nanotube was positioned at an angle of π/4 with respect to two polarizers. In the two different configurations, fast axis of the quarter-wave plate was kept at a small angle (θ) with polarizer 1 (Fig. 1b) or polarizer 2 (Fig. 1c) to generate left-handed (E_L) or right-handed (E_R) elliptical-polarization light as the excitation for the nanotube. Due to the very strong 1D depolarization effect, the nanotube scattering field is mainly polarized along the nanotube axial direction[35, 36]. Therefore, the nanotube forward scattering field can be written as $E_{NT}^{L}=\beta\tilde{\chi}E_L$ and $E_{NT}^{R}=\beta\tilde{\chi}E_R$ respectively, where β represents a scattering coefficient. Before polarizer 2, the forward-scattering light of the nanotube interferes with the transmitted optical reference beam (Fig. 1d and 1e), which yields the optical contrast signal as

$$\frac{\Delta T_{\mathrm{i}}}{T}=\frac{\left|E_{\mathrm{i}}+E_{\mathrm{NT}}^{\mathrm{i}}\right|^{2}-|E_{\mathrm{i}}|^{2}}{|E_{\mathrm{i}}|^{2}}\approx\frac{2Re\left(E_{\mathrm{i}}E_{\mathrm{NT}}^{\mathrm{i}*}\right)}{|E_{\mathrm{i}}|^{2}},\qquad(1)$$

where T_{i} is the transmission signal intensity, ΔT_{i} is the change of transmission signal intensity resulted from the presence of a nanotube, and i stands for L or R (The $|E_{\mathrm{NT}}^{\mathrm{i}}|^{2}$ term has been neglected because it is orders of magnitude smaller than the cross term). After polarizer 2, the reference light field is decreased dramatically due to small eccentricity of elliptically polarized light ($E_{\mathrm{o}}^{\mathrm{i}}=(E_{\mathrm{i}}\sin 2\theta)/\sqrt{2}$), while the nanotube's scattering field is only decreased by a small proportion ($E_{\mathrm{s}}^{\mathrm{i}}=E_{\mathrm{NT}}^{\mathrm{i}}/\sqrt{2}$). Therefore, the optical contrast is greatly enhanced, typically by 20 times in our transmission geometry. More importantly, the variation of the modulated signals depends on the real part of the cross term $E_{\mathrm{o}}^{\mathrm{i}}(E_{\mathrm{s}}^{\mathrm{i}})^{*}$, and this term varies with the elliptical chirality of incident light (Figs. 1f and 1g). In detail, detected optical contrast signals caused by left- or right-handed incident light can be written as:

$$\frac{\Delta T_{\mathrm{L}}}{T}=\alpha(\chi_{2}-\chi_{1}),\frac{\Delta T_{\mathrm{R}}}{T}=\alpha(\chi_{2}+\chi_{1}),\alpha=\frac{\beta}{\sin 2\theta}\,.\qquad(2)$$

Since χ_1 and χ_2, respectively, have the opposite and same contribution in the optical signal with left- and right-handed elliptically polarized excitation, the solution of both χ_1 and χ_2 can be obtained unambiguously (See more details in Supplementary Note 1).

Complex optical susceptibility measurement of individual suspended nanotube.

Scanning electron microscopic (SEM) image of a nanotube suspended across an open slit in SiO_2/Si substrate is shown in Fig. 2a. The chiral index of this nanotube was identified as (19, 11) from its electron diffraction pattern (Fig. 2b) and its Rayleigh scattering or absorption spectrum[37]. Fig 2c and 2d show optical contrast signals in photon energy range of 1.60-2.70 eV under left-

(Fig. 2c) and right-handed (Fig. 2d) elliptically polarized light excitation (θ= 2°). This set of spectra show two characteristic features, which are significantly different from absorption spectra[26]: (1) the peaks are not Lorentzian like, with slow bumps and pits; (2) optical contrast signal goes below zero at some energies. These features are originated from the opposite (same) contribution of χ_1 (χ_2) to the optical signal. According to Eq. 2, we extract the spectra of χ_1 (orange line) and χ_2 (green line) separately (Fig. 2e). The two optical resonances seat at 1.83 and 2.09 eV, corresponding to S_{33} and S_{44} optical transitions of the nanotube. The main peaks of χ_2 can be decomposed into the dominant exciton contribution and a continuum contribution (band-to-band transitions)[26]. The weak peak located at 2.3 eV above the main resonance is attributed to a phonon side band[38-40]. In addition to solving χ_1 and χ_2, the elliptical polarization excitation also enables the enhancement of the detected contrast signal as we accurately control the fast axis angle θ. When θ decreases from 4° to 1.4°, the detected signal (taking $\alpha\chi_1$ as an example) increases linearly with $1/\sin 2\theta$ (Fig. 2f and Supplementary Fig. 1), which is in accordance with the quantitative analysis of Eq. 2.

Systematical complex optical susceptibility measurement of individual nanotubes.

By estimating the scattering coefficient β in our experiment (See Supplementary Note 2), we can further give out the absolute value of $\tilde{\chi}$ for a nanotube. In total, 20 single-walled carbon nanotubes are measured (Supplementary Fig. 2) and three representative complex susceptibilities of them are shown in Fig. 3. From the electron diffraction patterns and optical transitions (Fig. 3a-c), these three nanotubes are identified as semiconducting (17, 12) and (13, 11) and metallic

(17, 17), respectively. Obviously, both χ_2 and χ_1 spectra (Fig. 3d-f) are intrinsic characteristics of a nanotube. As the ultralong nanotubes on open slits are typically with diameters of 1.5-3.0 nm, we can only access optical transitions higher than S_{22} in our laser spectral range of 1.6-2.7 eV. In principle, we can also measure E_{11} transition as long as one can grow the ultralong nanotubes with diameter less than 0.8 nm on the wide slit in the future.

According to Kramers-Kronig relation, the χ_1 can be obtained from χ_2 by

$$\chi_1(E) = \frac{2}{\pi}\int_0^{\infty} \frac{E'\chi_2(E')}{(E')^2 - E^2} dE'. \quad (3)$$

This integration requires the full energy data ranging from 0 eV to infinity of χ_2. Nevertheless, by utilizing the measured χ_2 data in energy range of 1.6-2.7 eV to perform K-K transformation, we can deduce a predicted χ_1^{KK} (Fig. 3d-f, gray lines). We found a relative good agreement between χ_1 and χ_1^{KK} around the resonance peak region, while obvious deviations in non-resonant region was observed. The agreement in the resonant region actually proves the accuracy of our measurement of χ_1, because the denominator weight factor around resonance region in Eq. 3 (E' is close to E) is very large and the ignorance of other non-resonant regions should still yield pretty good prediction. While the deviation in the non-resonant region highlights the necessity of independent χ_1 measurement other than predicted χ_1^{KK} since one could never obtain χ_2 in full energy region. The discrepancy can be understood from Eq.3. When conducting K-K transformation in a limited range of 1.6-2.7 eV, the influence of χ_2 spectra outside the range is not considered, resulting in an inaccurate calculated value of χ_1^{KK}. χ_2 below 1.6 eV gives a negative contribution to calculated χ_1^{KK}, while χ_2 above 2.7 eV gives a positive contribution. Therefore, the accurate distribution of those unconsidered optical transitions mainly determines

the deviation between χ_1 and χ_1^{KK}. In particular, the optical transitions are fingerprints of each nanotube with different chirality, therefore a simple K-K calculation from χ_2 of limited energy range in principle can't produce accurate χ_1^{KK} constantly.

On-chip complex optical susceptibility detection of individual nanotubes.

As for most optical applications in devices, nanotubes will be on substrates. Furtherly, we developed our technique for nanotubes on substrates in a reflection geometry (Fig. 4a). Compared with the transmission geometry, a reflection pre-factor $(1+r)^2/r$ is added to final contrast signal ($\alpha' = \alpha(1+r)^2/r$), where r is the reflection coefficient calculated from Fresnel equations and $1+r$ is the local field experienced by the nanotube (See more details in Supplementary Note 3). This will lead to even higher contrast signal enhancement to ~100 times, in contrast to the ~20 times enhancement for suspended nanotubes in the transmission geometry. In Fig. 4b, we show a representative measurement on semiconducting (25, 11) nanotubes with nice χ_1 and χ_2 spectra. Optical transition peaks identified from the extracted imaginary data were used to determine the nanotube chirality based on the atlas developed before[37]. Same as transmission spectrum, deduced χ_1^{KK} agrees with the experimental value around the resonance peak region (See Supplementary Fig. 3).

Discussion

An advantage of carbon nanotubes for optical application is the well-defined atomic structure and associated optical transitions that can be accurately described by both theory and experimental data base[37]. From our $\tilde{\chi}$ measurement, we can clearly see that every nanotube has different χ_1

and χ_2 value at different energy region, which is a great advantage in the nanophononics, including but not limited to metasurfaces. With the spatial control of the $\tilde{\chi}$-determined nanotubes, one can readily tailor the wave fronts of light beams with arbitrary phase, polarization and amplitude distributions, which holds a great promise to implement the subwavelength optical components[41], optical computation[42] and information processing[43], whilst, enjoys merits of the low loss and reduced dimension because the 1D nature of nanotubes. Further, nanotube can have different walls, such as single wall and double walls with more optical transitions (See Supplementary Fig. S4), and the richness and flexibility in the optical engineering for meta-materials application are therefore very promising[44].

In summary, the direct measurement of the basic complex optical susceptibility of 1D materials is obviously fundamental for their accurate design and applications in the future photonic, optoelectronic, photovoltaic and bio-imaging devices, provides a new detectable parameter to monitor the external regulations such as charge doping, strain, molecular adsorption, and dielectric environment, and will further evoke theoretical understanding of 1D physics by complex susceptibility. The signal detection limit of our technique is estimated to be ~10^{-6} (See Supplementary Note 4). This high sensitivity can ensure the detection of nanotubes with the smallest diameter down to 0.3 nm. Thus, for general 1D materials with defined structure, such as long graphene nanoribbons and semiconductor nanowires, our technique is ready to work as well.

Methods

Nanotube preparation. In this study, nanotubes were grown by chemical vapor deposition (CVD) method. We used ethanol through argon bubble as carbon precursor and a thin ion film (0.2 nm) as catalyst for the synthesis at 950℃ for 30 min. Suspended SWNTs were grown across open slit structures on Si/SiO_2 substrate.

TEM characterization. Electron diffraction patterns were obtained in TEM (JEOL 2100 and ARM 3000) under 80 keV. Electron beam and laser beam can both go through the open slit with individual carbon nanotubes, which enables directly investigation of the chiral indices and optical spectrum of the same nanotubes.

Optical setup. For transmission configuration (Fig. 1a), optical signal was collected by a home-built confocal microscope system, where a supercontinuum laser (Fianium SC-400-4) is used as the light source, shooting light through polarizer 1 (Thorlabs, GTH10M) and a quarter-wave plate (Thorlabs, AQWP05M-600A). Then an objective (Mitutoyo M Plan 50 X, NA = 0.42) serves to focus the light to the sample and another objective (Mitutoyo M Plan 50 X, NA = 0.42) collects the transmitted light. An oblique objective (Mitutoyo M Plan 50 X, NA = 0.42) was used to collect nanotube's scattering signal to a CCD camera (PULNIX TM-7CN) for Rayleigh imaging. The transmission signal was modulated by polarizer 2 (Thorlabs, GTH10M). Two sets of spectra with the nanotube in and out of the beam focus were obtained to generate the contrast spectra by a spectrometer containing a grating (Thorlabs, GT50-03) and a linear CCD (Imaging Solution Group, LW ELIS-1024a-1394). In the reflection geometry (Fig. 4a), the main difference is the use of a beam splitter (customer-polished quartz glass) and only one objective (Nikon S Plan Fluor 40 X, NA = 0.65).

References:

1. Saito, R., Fujita, M., Dresselhaus, G. & Dresselhaus, M.S. Electronic-Structure of Chiral Graphene Tubules. *Appl Phys Lett* **60**, 2204-2206 (1992).
2. Kataura, H., Kumazawa, Y., Maniwa, Y., Umezu, I., Suzuki, S. et al. Optical properties of single-wall carbon nanotubes. *Synthetic Met* **103**, 2555-2558 (1999).
3. Bachilo, S.M., Strano, M.S., Kittrell, C., Hauge, R.H., Smalley, R.E. et al. Structure-assigned optical spectra of single-walled carbon nanotubes. *Science* **298**, 2361-2366 (2002).
4. Ando, T. Excitons in carbon nanotubes. *J Phys Soc Jpn* **66**, 1066-1073 (1997).
5. Maultzsch, J., Pomraenke, R., Reich, S., Chang, E., Prezzi, D. et al. Exciton binding energies in carbon nanotubes from two-photon photoluminescence. *Phys Rev B* **72**, 241402 (2005).
6. Wang, F., Dukovic, G., Brus, L.E. & Heinz, T.F. The optical resonances in carbon nanotubes arise from excitons. *Science* **308**, 838-841 (2005).
7. Matsunaga, R., Matsuda, K. & Kanemitsu, Y. Evidence for dark excitons in a single carbon nanotube due to the Aharonov-Bohm effect. *Phys Rev Lett* **101**, 147404 (2008).
8. Colombier, L., Selles, J., Rousseau, E., Lauret, J.S., Vialla, F. et al. Detection of a biexciton in semiconducting carbon nanotubes using nonlinear optical spectroscopy. *Phys Rev Lett* **109**, 197402 (2012).
9. Stich, D., Spath, F., Kraus, H., Sperlich, A., Dyakonov, V. et al. Triplet-triplet exciton dynamics in single-walled carbon nanotubes. *Nat Photonics* **8**, 139-144 (2014).
10. Gabor, N.M., Zhong, Z.H., Bosnick, K., Park, J. & McEuen, P.L. Extremely Efficient Multiple Electron-Hole Pair Generation in Carbon Nanotube Photodiodes. *Science* **325**, 1367-1371 (2009).
11. Chen, J., Perebeinos, V., Freitag, M., Tsang, J., Fu, Q. et al. Bright infrared emission from electrically induced excitons in carbon nanotubes. *Science* **310**, 1171-1174 (2005).
12. Wang, F., Rozhin, A.G., Scardaci, V., Sun, Z., Hennrich, F. et al. Wideband-tuneable nanotube mode-locked fibre laser. *Nat Nanotechnol* **3**, 738-742 (2008).
13. Ma, X., Hartmann, N.F., Baldwin, J.K., Doorn, S.K. & Htoon, H. Room-temperature single-

photon generation from solitary dopants of carbon nanotubes. *Nat Nanotechnol* **10**, 671-675 (2015).

14. Graf, A., Held, M., Zakharko, Y., Tropf, L., Gather, M.C. et al. Electrical pumping and tuning of exciton-polaritons in carbon nanotube microcavities. *Nat Mater* **16**, 911-917 (2017).
15. Avouris, P., Freitag, M. & Perebeinos, V. Carbon-nanotube photonics and optoelectronics. *Nat Photonics* **2**, 341-350 (2008).
16. Sharma, A., Singh, V., Bougher, T.L. & Cola, B.A. A carbon nanotube optical rectenna. *Nat Nanotechnol* **10**, 1027-1032 (2015).
17. Pyatkov, F., Futterling, V., Khasminskaya, S., Flavel, B.S., Hennrich, F. et al. Cavity-enhanced light emission from electrically driven carbon nanotubes. *Nat Photonics* **10**, 420-427 (2016).
18. Dang, X., Yi, H., Ham, M.H., Qi, J., Yun, D.S. et al. Virus-templated self-assembled single-walled carbon nanotubes for highly efficient electron collection in photovoltaic devices. *Nat Nanotechnol* **6**, 377-384 (2011).
19. Barone, P.W., Baik, S., Heller, D.A. & Strano, M.S. Near-infrared optical sensors based on single-walled carbon nanotubes. *Nat Mater* **4**, 86-92 (2005).
20. Heinz, T.F. Rayleigh scatteing spectroscopy. *Carbon Nanotubes* **111**, 353-369 (Springer, 2007).
21. Malic, E., Hirtschulz, M., Milde, F., Wu, Y., Maultzsch, J. et al. Theory of Rayleigh scattering from metallic carbon nanotubes. *Phys Rev B* **77**, 045432 (2008).
22. Fujiwara, H. Spectroscopic ellipsometry: principles and applications (John Wiley & Sons, 2007).
23. Shen, Y.-R. The principles of nonlinear optics. *New York, Wiley-Interscience, 1984* (1984).
24. Berciaud, S., Cognet, L., Poulin, P., Weisman, R.B. & Lounis, B. Absorption spectroscopy of individual single-walled carbon nanotubes. *Nano Lett* **7**, 1203-1207 (2007).
25. Blancon, J.C., Paillet, M., Tran, H.N., Than, X.T., Guebrou, S.A. et al. Direct measurement of the absolute absorption spectrum of individual semiconducting single-wall carbon

nanotubes. *Nat Commun* **4**, 2542 (2013).

26. Liu, K.H., Hong, X.P., Choi, S., Jin, C.H., Capaz, R.B. et al. Systematic determination of absolute absorption cross-section of individual carbon nanotubes. *PNAS* **111**, 7564-7569 (2014).
27. Lindfors, K., Kalkbrenner, T., Stoller, P. & Sandoghdar, V. Detection and spectroscopy of gold nanoparticles using supercontinuum white light confocal microscopy. *Phys Rev Lett* **93**, 037401 (2004).
28. Bohren, C.F. & Huffman, D.R. Absorption and scattering of light by small particles (John Wiley & Sons, 2008).
29. Jan, C.M., Lee, Y.H., Wu, K.C. & Lee, C.K. Integrating fault tolerance algorithm and circularly polarized ellipsometer for point-of-care applications. *Opt Express* **19**, 5431-5441 (2011).
30. Sherson, J.F., Krauter, H., Olsson, R.K., Julsgaard, B., Hammerer, K. et al. Quantum teleportation between light and matter. *Nature* **443**, 557-560 (2006).
31. Mak, K.F., McGill, K.L., Park, J. & McEuen, P.L. The valley Hall effect in MoS_2 transistors. *Science* **344**, 1489-1492 (2014).
32. Yoshikawa, N., Tamaya, T. & Tanaka, K. High-harmonic generation in graphene enhanced by elliptically polarized light excitation. *Science* **356**, 736-738 (2017).
33. Lefebvre, J. & Finnie, P. Polarized light microscopy and spectroscopy of individual single-walled carbon nanotubes. *Nano Res* **4**, 788-794 (2011).
34. Liu, K., Hong, X., Zhou, Q., Jin, C., Li, J. et al. High-throughput optical imaging and spectroscopy of individual carbon nanotubes in devices. *Nat Nanotechnol* **8**, 917-922 (2013).
35. Islam, M.F., Milkie, D.E., Kane, C.L., Yodh, A.G. & Kikkawa, J.M. Direct measurement of the polarized optical absorption cross section of single-wall carbon nanotubes. *Phys Rev Lett* **93**, 037404 (2004).
36. Murakami, Y., Einarsson, E., Edamura, T. & Maruyama, S. Polarization dependence of the optical absorption of single-walled carbon nanotubes. *Phys Rev Lett* **94**, 087402 (2005).

37. Liu, K., Deslippe, J., Xiao, F., Capaz, R.B., Hong, X. et al. An atlas of carbon nanotube optical transitions. *Nat Nanotechnol* **7**, 325-329 (2012).
38. Htoon, H., O'Connell, M.J., Doorn, S.K. & Klimov, V.I. Single carbon nanotubes probed by photoluminescence excitation spectroscopy: the role of phonon-assisted transitions. *Phys Rev Lett* **94**, 127403 (2005).
39. Chou, S.G., Plentz, F., Jiang, J., Saito, R., Nezich, D. et al. Phonon-assisted excitonic recombination channels observed in DNA-wrapped carbon nanotubes using photoluminescence spectroscopy. *Phys Rev Lett* **94**, 127402 (2005).
40. Perebeinos, V., Tersoff, J. & Avouris, P. Electron-phonon interaction and transport in semiconducting carbon nanotubes. *Phys Rev Lett* **94**, 086802 (2005).
41. Yu, N.F., Genevet, P., Kats, M.A., Aieta, F., Tetienne, J.P. et al. Light Propagation with Phase Discontinuities: Generalized Laws of Reflection and Refraction. *Science* **334**, 333-337 (2011).
42. Hwang, Y. & Davis, T.J. Optical metasurfaces for subwavelength difference operations. *Appl Phys Lett* **109**, 181101 (2016).
43. Huang, L.L., Chen, X.Z., Muhlenbernd, H., Zhang, H., Chen, S.M. et al. Three-dimensional optical holography using a plasmonic metasurface. *Nat Commun* **4**, 2808 (2013).
44. Liu, K.H., Jin, C.H., Hong, X.P., Kim, J., Zettl, A. et al. Van der Waals-coupled electronic states in incommensurate double-walled carbon nanotubes. *Nat Phys* **10**, 737-742 (2014).

Acknowledgments

The authors thank for fruitful discussion with Wentao Yu, Dongxue Chen and Feng Yang. This work was supported by National Key R&D Program of China (2016YFA0300903, 2016YFA0200103), NSFC (51522201 and 11474006), National Equipment Program of China (ZDYZ2015-1), Beijing Graphene Innovation Program (Z161100002116028), Guangdong Innovative and Entrepreneurial Research Team Program (2016ZT06D348), Science Technology and Innovation Commission of Shenzhen Municipality (ZDSYS20170303165926217 and JCYJ20170412152620376), and the National Program for Thousand Young Talents of China.

Author contributions

K.L. and F.Y. conceived the project. K.L., F.W., E.W., D.Y. supervised the project. F.Y. and K.L. performed optical experiments. C.L., Q.Z., S.Z., M.W., and J.Z. grew the carbon nanotubes. C.C., F.Y. and J.L. performed theoretical analysis. K.L., F.Y., F.X, J.Z., S.M. and Z.S. analyzed the experimental data. K.L., P.G. and X.B. carried out the TEM experiments. All of the authors discussed the results and wrote the paper.

Additional information:

Supplementary Information accompanies this paper at http://www.nature.com/-naturecommunications

Competing financial interests: The authors declare no competing financial interests.

Reprints and permission information is available online at http://npg.nature.com/-reprintsandpermissions/

Figure captions

Figure 1 | Scheme of complex optical susceptibility measurement in a transmission geometry. **a,** Scheme of experiment setup. Two polarizers were strictly perpendicular to each other. A quarter-wave plate was used to generate the elliptical chirality (left- or right-handed). A vertically placed carbon nanotube was put at the focus of the two confocal objectives. **b-c,** Layouts of the polarization control and the nanotube. The nanotube was laid at the bisector of the two polarizers' axis. The fast axis of the wave plate was kept at a small angle (θ) to the polarizer axis. **d-e,** Interference scheme of input left- (E_{L}) and right-handed (E_{R}) elliptically polarized light and nanotube forward-scattering field ($E_{\mathrm{NT}}^{\mathrm{L}}$ or $E_{\mathrm{NT}}^{\mathrm{R}}$). **f-g,** Illustrations of complex phase diagrams of the detected optical contrast signal with left/right elliptically polarized light excitation after polarizer 2, in which χ_1 contributes oppositely under two layouts.

Figure 2 | Complex optical susceptibility measurement of individual suspended nanotube. a, Scanning electron micrograph (SEM) image of a suspended carbon nanotube across an open slit etched on SiO_2/Si substrate. **b,** The electron diffraction pattern reveals the chiral index of nanotube as (19, 11), a semiconducting tube with a diameter of 2.06 nm. **c-d,** Optical contrast spectra with left- (E_{L}) (**c**) and right-handed (E_{R}) (**d**) elliptically polarized excitation. The angle θ between the wave plate and polarizer 1 or 2 is set as 2°. **e,** Real ($\alpha\chi_1$, orange line) and imaginary ($\alpha\chi_2$, green line) susceptibility of the nanotube under $\theta = 2°$. The two peaks are corresponded to S_{33} and S_{44} optical transitions, respectively. **f,** Dependence of detected real susceptibility value ($\alpha\chi_1$) on θ. With θ increasing from 1.4° to 4°, the signal decreases linearly with $1/\sin 2\theta$ (Supplementary Fig. 1). α is a detection coefficient.

Figure 3 | Systematical complex optical susceptibility measurement of individual nanotubes. **a-c,** Electron diffraction patterns of three single-walled carbon nanotubes with different chiral indices. The (17, 12) semiconducting nanotube (**a**) has a diameter of 1.98 nm; the (13,11) semiconducting nanotube (**b**) has a diameter of 1.63 nm; the (17,17) metallic nanotube (**c**) has a diameter of 2.31 nm. **d-f,** Measured imaginary (χ_2, green) and real (χ_1, orange) susceptibility of nanotubes in **a**–**c** under $\theta = 2°$. The calculated real susceptibility (χ_1^{KK}, gray) through Kramers-Kronig transformation of χ_2 in a finite photon energy range (1.6-2.7 eV) were also shown. A good agreement between χ_1 and χ_1^{KK} is achieved around the resonance peak region, while obvious deviation can happen in non-resonant region. Optical transitions are marked above each peak.

Figure 4 | On-chip complex optical susceptibility detection of individual nanotubes. **a,** Scheme of the experiment setup in the reflection configuration. **b,** Imaginary (χ_2, green) and real (χ_1, orange) susceptibilities of nanotube (25,11) on fused quartz substrate. α' is a detection coefficient. Optical transitions are marked above each peak. S_{55} and S_{66} transitions are very close with each other.

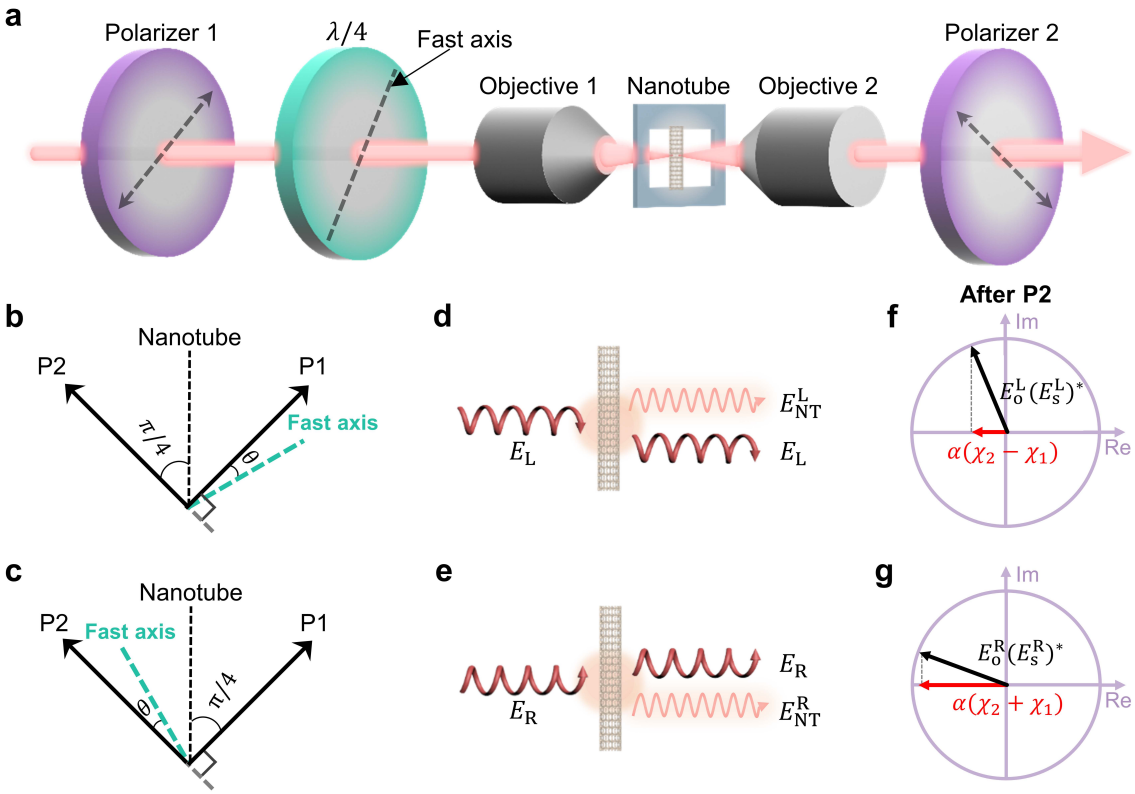
a
Polarizer 1
λ/4
Fast axis
Objective 1
Nanotube
Objective 2
Polarizer 2
b
Nanotube
P2
P1
π/4
θ
Fast axis
c
Nanotube
P2
Fast axis
P1
θ
π/4
d
E_{L}
$E_{\mathrm{NT}}^{\mathrm{L}}$
E_{L}
e
E_{R}
E_{R}
$E_{\mathrm{NT}}^{\mathrm{R}}$
f
After P2
Im
Re
$E_{\mathrm{o}}^{\mathrm{L}}(E_{\mathrm{s}}^{\mathrm{L}})^{*}$
$\alpha(\chi_2-\chi_1)$
g
Im
Re
$E_{\mathrm{o}}^{\mathrm{R}}(E_{\mathrm{s}}^{\mathrm{R}})^{*}$
$\alpha(\chi_2+\chi_1)$

Figure 1

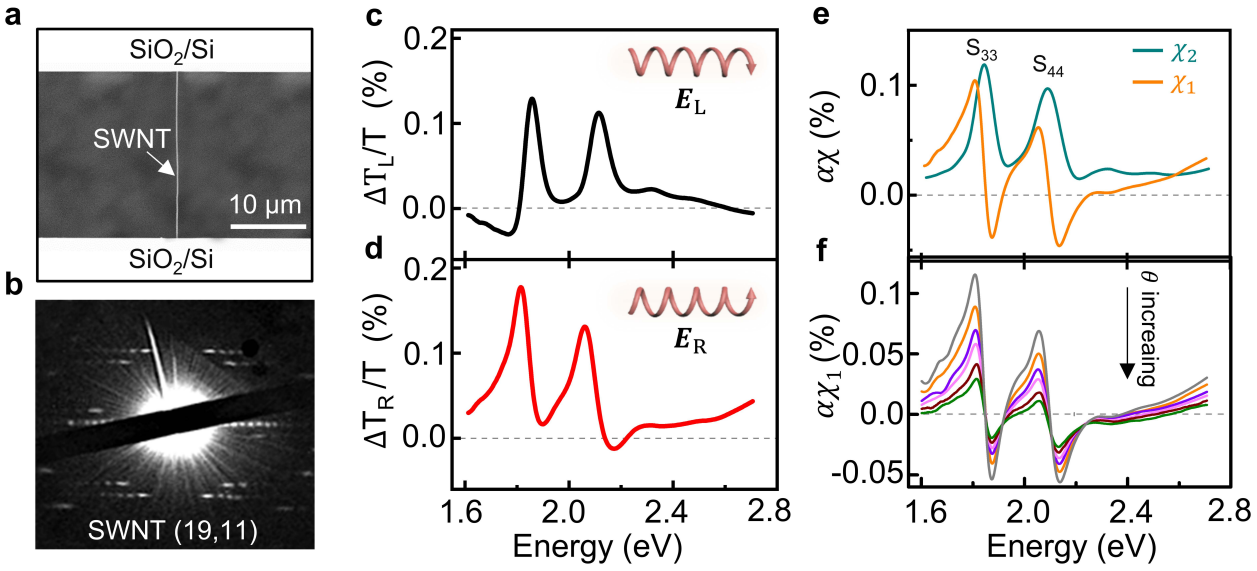
a
SiO2/Si
SWNT
10 μm
SiO2/Si
b
SWNT (19,11)
c
ΔTL/T (%)
EL
d
ΔTR/T (%)
ER
Energy (eV)
e
S33
S44
χ2
χ1
αχ (%)
f
αχ1 (%)
θ increaing
Energy (eV)

Figure 2

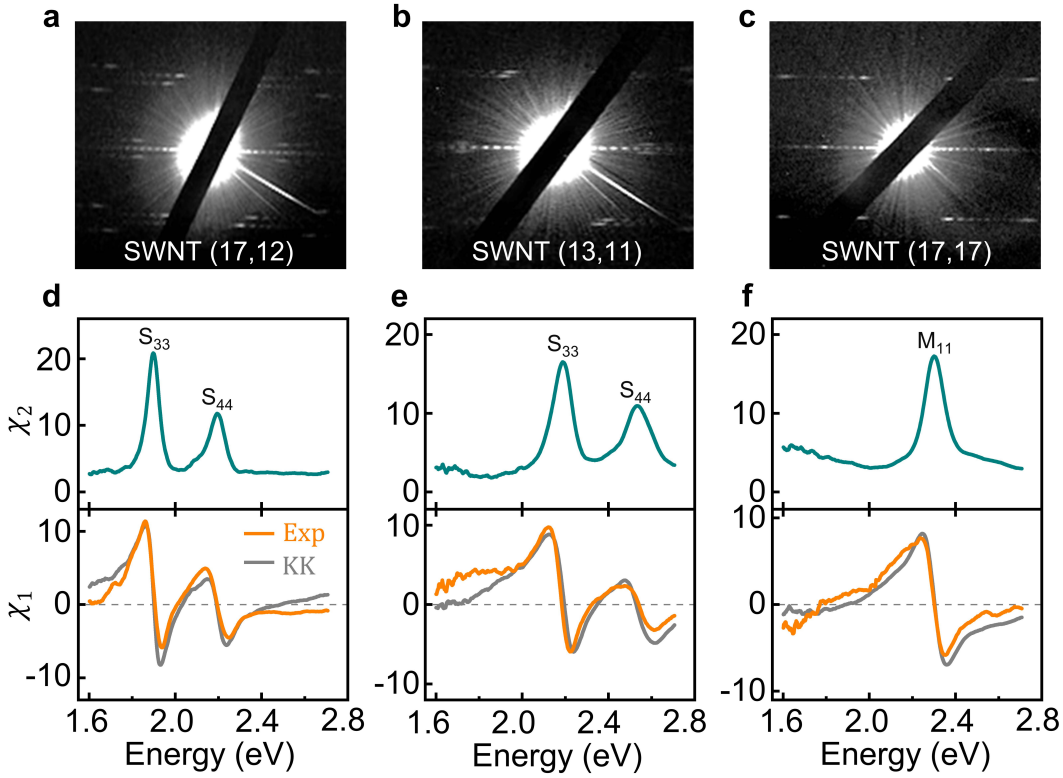
a
b
c
SWNT (17,12)
SWNT (13,11)
SWNT (17,17)
d
e
f
S33
S44
M11
χ2
χ1
Exp
KK
20
10
0
-10
1.6
2.0
2.4
2.8
Energy (eV)

Figure 3

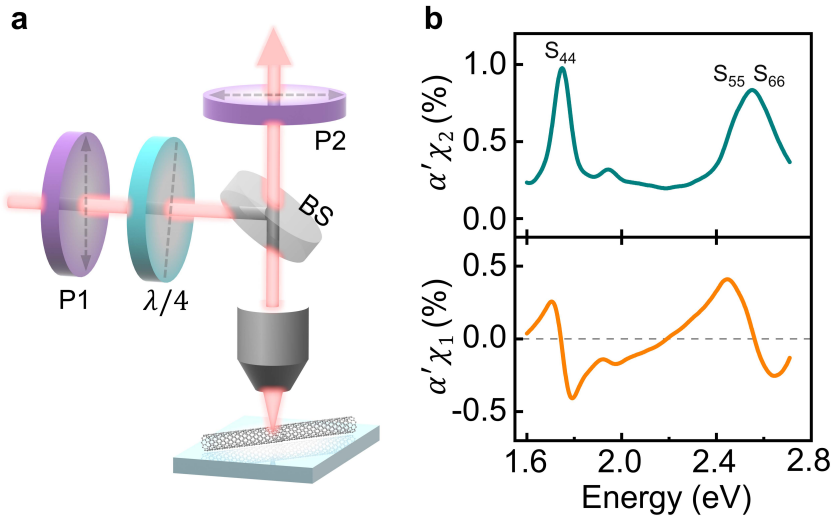
a
P2
BS
P1
λ/4
b
S44
S55 S66
1.0
0.5
0.0
α′χ2 (%)
0.5
0.0
-0.5
α′χ1 (%)
1.6
2.0
2.4
2.8
Energy (eV)

Figure 4

Supplementary Material

Measurement of Complex Optical Susceptibility for Individual Carbon Nanotubes by Elliptically Polarized Light Excitation

Fengrui Yao, Can Liu, Cheng Chen, Shuchen Zhang, Qiuchen Zhao, Fajun Xiao, Muhong Wu, Jiaming Li, Peng Gao, Jianlin Zhao, Xuedong Bai, Shigeo Maruyama, Dapeng Yu, Enge Wang, Zhipei Sun, Jin Zhang, Feng Wang and Kaihui Liu*

The supplementary information includes:

Supplementary Figure 1-5

Supplementary Note 1-4

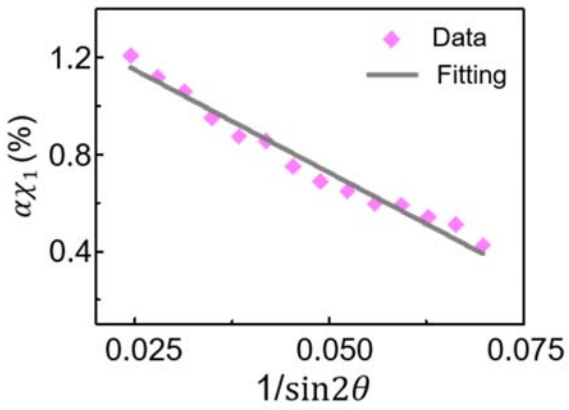

Supplementary Fig. 1: Angle θ dependent signal ($\alpha\chi_1$) at photon energy of 1.81 eV. Linear dependence on $1/\sin 2\theta$ is shown.

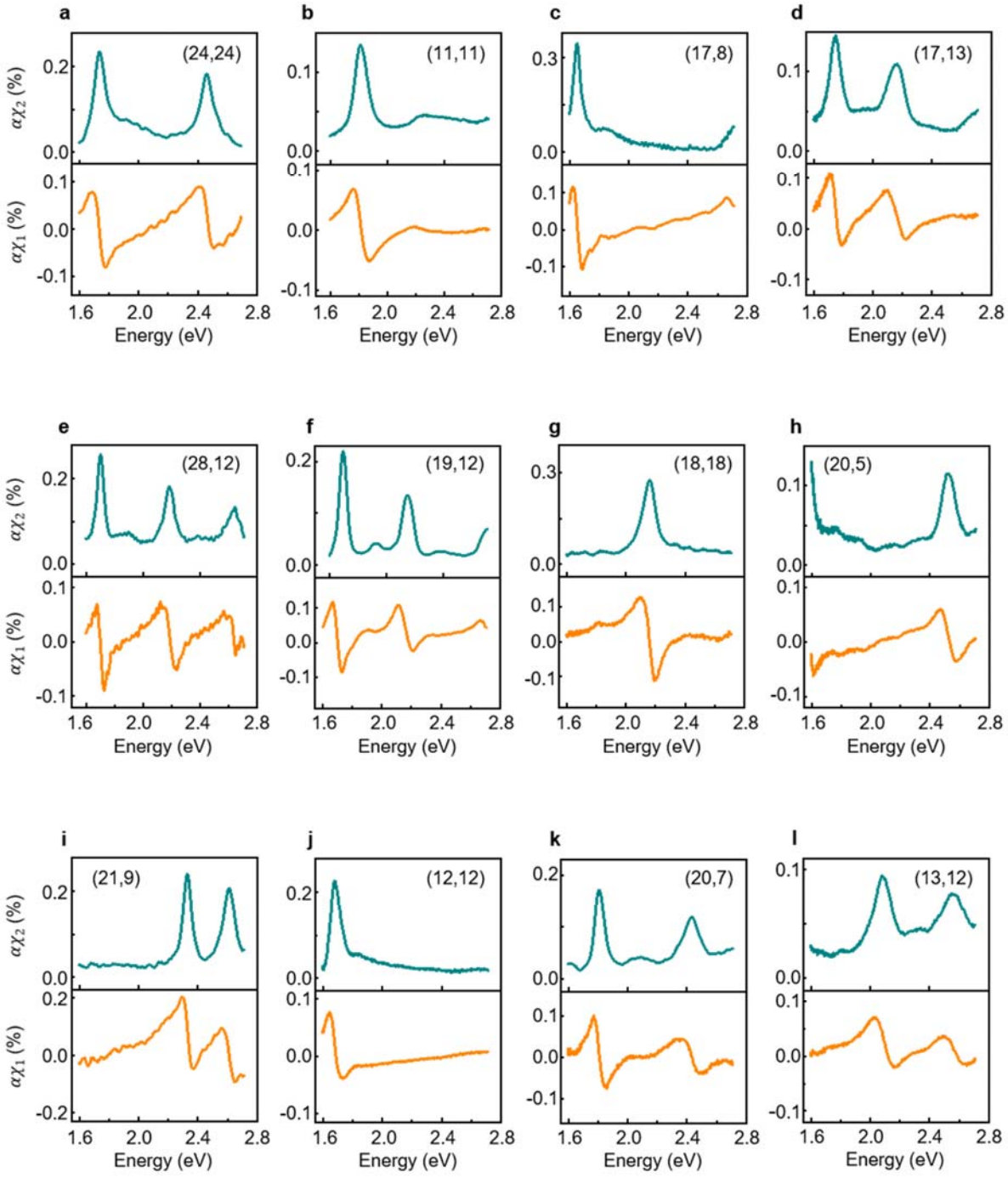
a
(24,24)
b
(11,11)
c
(17,8)
d
(17,13)
e
(28,12)
f
(19,12)
g
(18,18)
h
(20,5)
i
(21,9)
j
(12,12)
k
(20,7)
l
(13,12)
$\alpha\chi_2$ (%)
$\alpha\chi_1$ (%)
Energy (eV)

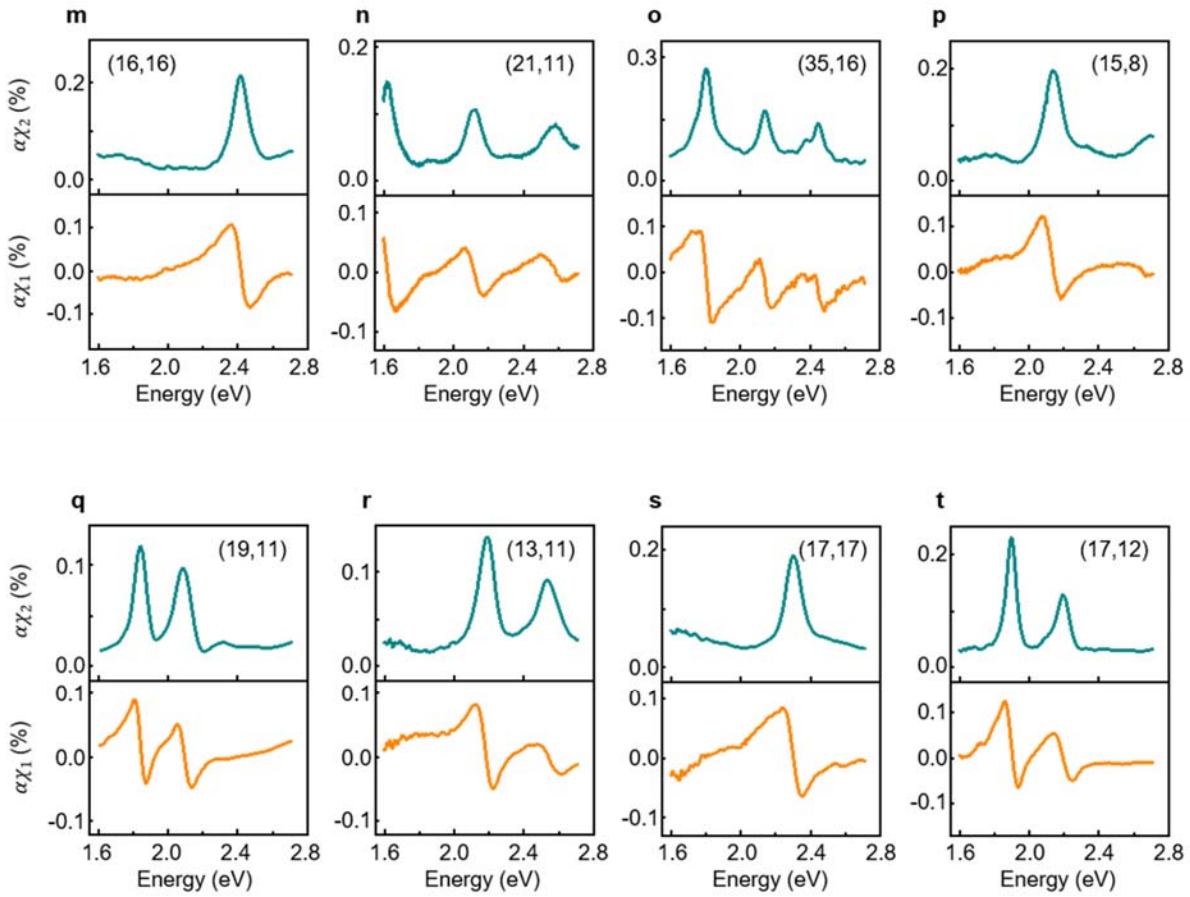

Supplementary Fig. 2: Measured imaginary (χ_2, green) and real (χ_1, orange) susceptibility of 20 SWNTs with different chiral indices. Determination of chirality was based on the electron diffraction pattern or the atlas of nanotube optical transitions[1]. The accuracy of the mesurement was further confirmed by converting the measured imaginary susceptiblity data to absolute absorption cross-sections, the average value of which converges on the graphene value[2].

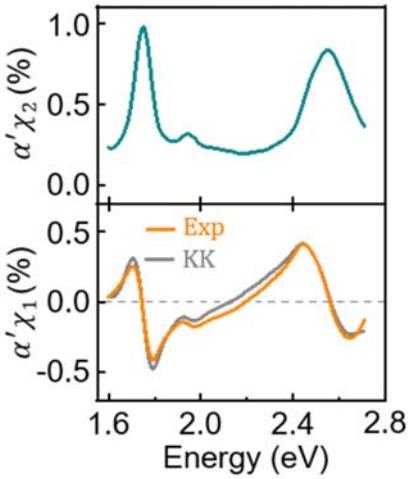

Supplementary Fig. 3: Imaginary (χ_2, green) and real (χ_1, orange) susceptibilities of nanotube (25,11) on fused quartz substrate. α' is a detection coefficient. The calculated real susceptibility (χ_1^{KK}, gray) through Kramers-Kronig transformation of χ_2 in a finite photon energy range (1.6-2.7 eV) was also shown.

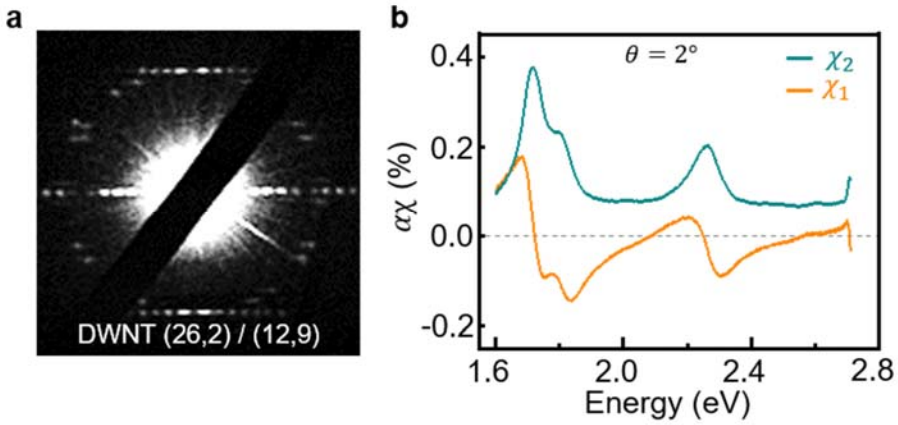

Supplementary Fig. 4: Complex optical susceptibility measurement of individual double-walled carbon nanotube (DWNT). a, Electron diffraction pattern of DWNT (26,2)/(12,9). The outer (inner) tube is metallic with a diameter of 2.12 (1.43) nm. **b**, Complex susceptibility of the same DWNT. The two resonances at 1.68 and 1.72 eV of χ_2 (green line) correspond to the M_{11}^- and M_{11}^+ electronic transitions of outer tube (26, 2), and the resonances at 2.20 eV correspond to the M_{22}^- electronic transitions of inter tube (12, 9)[1]. The angle θ between the waveplate and polarizer 1 or polarizer 2 is kept at 2 ° for this measurement.

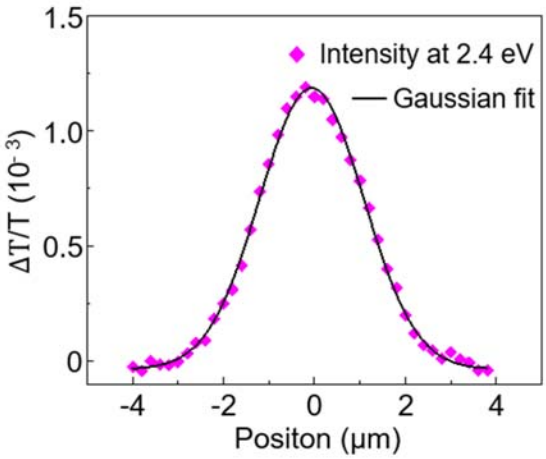

Supplementary Fig. 5: Dependence of contrast signal at 2.4 eV on nanotube's position in the beam focus and its fitting to Gaussian function of Eq. S8.

Supplementary Note 1. Extract real and imaginary part of complex optical susceptibility from the transmission homodyne modulation signal.

In the first case, to generate a left-handed elliptically polarized light, we kept the angle between the quarter-wave plate and the first polarizer (P1) at θ. Let E_{in} denote the electric field of the incident light after P1. Modulated by a quarter-wave plate, the local field experienced by the nanotube in this case would be left-handed, with the expression: $\boldsymbol{E}_{\mathrm{L}} = E_{\mathrm{in}}\mathrm{e}^{-\mathrm{i}\frac{\pi}{2}}\cos\theta\boldsymbol{i} + E_{\mathrm{in}}\sin\theta\boldsymbol{j}$, where $\boldsymbol{i}$ and $\boldsymbol{j}$ are unit vectors along the fast and slow axis of the quarter-wave plate, respectively, and $\mathrm{e}^{-\mathrm{i}\frac{\pi}{2}}$ denotes the phase difference between the fast and slow axis of the quarter-wave plate. The first term is the electric field along the fast axis, while the second term is that along the slow axis. Then the transmitting light after P2 ($E_{\mathrm{o}}^{\mathrm{L}}$) is

$$E_{\mathrm{o}}^{\mathrm{L}} = \mathrm{e}^{-\mathrm{i}\frac{\pi}{2}}E_{\mathrm{in}}(\mathrm{e}^{-\mathrm{i}\frac{\pi}{2}}\cos\theta\sin\theta - \sin\theta\cos\theta) = (\mathrm{i}-1)E_{\mathrm{in}}\sin\theta\cos\theta. \quad (1)$$

Where the first $e^{-\mathrm{i}\frac{\pi}{2}}$ term is caused by Gouy's phase shift, and the second $e^{-\mathrm{i}\frac{\pi}{2}}$ term is from the phase difference between the fast and slow axis of a quarter-wave plate. The nanotube scattering electric field is polarized along the nanotube direction due to its strong depolarization effect, the scattering field (E_{NT}) amplitude would be

$$E_{\mathrm{NT}}^{\mathrm{L}} = \beta\tilde{\chi}E_{\mathrm{L}} = \beta\tilde{\chi}E_{\mathrm{in}}\left[\mathrm{e}^{-\mathrm{i}\frac{\pi}{2}}\cos\theta\cos\left(\frac{\pi}{4}+\theta\right) + \sin\theta\cos\left(\frac{\pi}{4}-\theta\right)\right]. \quad (2)$$

Here β represents an efficiency coefficient (details in Supplementary Note 2). Then, we could derive the nanotube scattering field after P2 ($E_{\mathrm{s}}^{\mathrm{L}}$) as

$$E_{\mathrm{s}}^{\mathrm{L}} = \beta\tilde{\chi}E_{\mathrm{in}}\left[\mathrm{e}^{-\mathrm{i}\frac{\pi}{2}}\cos\theta\cos\left(\frac{\pi}{4}+\theta\right)\cos\frac{\pi}{4} + \sin\theta\cos\left(\frac{\pi}{4}-\theta\right)\cos\frac{\pi}{4}\right]. \quad (3)$$

Based on equation (1) and (3), we could derive that:

$$\frac{\Delta T_L}{T} = \frac{2\mathrm{Re}\left(E_o^L (E_s^L)^*\right)}{\left|E_o^L\right|^2} = \frac{\beta\chi_2(\cos 2\theta - \sin 2\theta)}{\sin 2\theta} - \frac{\beta\chi_1}{\sin 2\theta} \approx \frac{\beta(\chi_2 - \chi_1)}{sin 2\theta}. \quad (4)$$

The approximation at last is reasonable because θ is set as a small angle ($\theta \leq 4°$).

In the second case, to generate a right-handed elliptically polarized light, we keep the angle between the wave plate and the second polarizer (P2) at θ. In this case, the local field would become right-handed, written as $\boldsymbol{E}_R = E_{in}\cos\theta \boldsymbol{i} + E_{in} e^{-i\frac{\pi}{2}} \sin\theta \boldsymbol{j}$, where $\boldsymbol{i}$ and $\boldsymbol{j}$ are the same unit vectors as we defined before. (Note that $\boldsymbol{i}$ and $\boldsymbol{j}$ do not change when rotating the orientation of the wave plate.) Similar to the previous case, we have

$$E_o^R = e^{-i\frac{\pi}{2}} E_{in}(-e^{-i\frac{\pi}{2}}\cos\theta\sin\theta + \sin\theta\cos\theta) = (1 - i)E_{in}\sin\theta\cos\theta \quad (5)$$

$$E_s^R = \beta\tilde{\chi}E_{in}\left[e^{-i\frac{\pi}{2}}\cos\theta\cos\left(\frac{\pi}{4} + \theta\right)\cos\frac{\pi}{4} + \sin\theta\cos\left(\frac{\pi}{4} - \theta\right)\cos\frac{\pi}{4}\right]. \quad (6)$$

Where E_o^R represents the transmitting light field after P2, E_s^R represents the nanotube scattering field after P2 in this case. Then we could derive

$$\frac{\Delta T_R}{T} = \frac{2\mathrm{Re}\left(E_o^R (E_s^R)^*\right)}{\left|E_o^R\right|^2} = \frac{\beta\chi_1}{\sin 2\theta} + \frac{\beta\chi_2(\cos 2\theta - \sin 2\theta)}{\sin 2\theta} \approx \frac{\beta(\chi_2 + \chi_1)}{\sin 2\theta}. \quad (7)$$

Supplementary Note 2. Determine the efficiency constant β

The supercontinuum with a Gaussian spatial profile can be described as

$$E(x,y) = E_0 e^{-\frac{(x-x_c)^2+(y-y_c)^2}{R^2}}. \quad (8)$$

Where x_c and y_c are the coordinates of the center position of the focus and R is a measure of the beam size. So energy density function of laser can be described as

$$I(x,y) = I_0 e^{-\frac{2(x-x_c)^2+2(y-y_c)^2}{R^2}}. \quad (9)$$

For a 1D nanotube (with a small diameter d) along y direction and positioned at x, the ratio between the total scattering intensity and incident light intensity over the nanotube length is[2-5]

$$\frac{(E_{NT}^i)^2}{(E_i)^2} = \frac{\int_{-\infty}^{\infty} \eta_1 \cdot \sigma \cdot e^{-\frac{2(x-x_c)^2+2(y-y_c)^2}{R^2}} dy \cdot \eta_2}{\int_{-\infty}^{\infty}\int_{-\infty}^{\infty} e^{-\frac{2(x-x_c)^2+2(y-y_c)^2}{R^2}} dxdy}$$

$$\approx \frac{e^{-\frac{2(x-x_c)^2}{R^2}} \cdot \sigma}{\frac{\sqrt{2\pi}R}{2}} \cdot \eta_1 \cdot \eta_2 = \eta_1 \cdot \eta_2 \cdot \sqrt{\frac{2}{\pi}} \cdot \frac{\sigma}{R} \cdot e^{-\frac{2(x-x_c)^2}{R^2}}. \quad (10)$$

Where η_1 is the excitation efficiency (about $1/\sqrt{2}$), η_2 is the collection efficiency of objective, σ is the scattering cross-section per unit length[4, 5] and it has the form of

$$\sigma(\omega) = \frac{\pi^2}{64c^3} d^4 \omega^3 |\tilde{\chi}(\omega)|^2. \quad (11)$$

Here ω is the angular frequency of light, c is the speed of light and d is the diameter of nanotube. With above equations, we obtain quantitative value of the β as

$$\beta = \sqrt{\frac{\pi^{3/2} d^4 \omega^3 \eta_1 \eta_2}{32\sqrt{2}c^3 R} e^{-\frac{2(x-x_c)^2}{R^2}}}. \quad (12)$$

Supplementary Note 3. Extract real and imaginary part of complex optical susceptibility from the reflection homodyne modulation signal.

The substrate-reflected field ($E_{\mathrm{o}}^{\mathrm{L}}$) and nanotube-scattered field ($E_{\mathrm{s}}^{\mathrm{L}}$) would be

$$E_{\mathrm{o}}^{\mathrm{L}} = rE_{\mathrm{in}}\mathrm{e}^{-\mathrm{i}\frac{\pi}{2}}(\mathrm{e}^{-\mathrm{i}\frac{\pi}{2}}\cos\theta\sin\theta - \sin\theta\cos\theta) = r(\mathrm{i}-1)E_{\mathrm{in}}\sin\theta\cos\theta \quad (13)$$

$$E_{\mathrm{s}}^{\mathrm{L}} = (1+r)^2\beta\tilde{\chi}E_{\mathrm{in}}\left[\mathrm{e}^{-\mathrm{i}\frac{\pi}{2}}\sin\theta\cos\left(\frac{\pi}{4}-\theta\right)\cos\frac{\pi}{4} + \cos\theta\cos\left(\frac{\pi}{4}+\theta\right)\cos\frac{\pi}{4}\right]. \quad (14)$$

Where r represents the reflection coefficient calculated from Fresnel equations and $1+r$ represents the local field experienced by the nanotube.

Then we could derive

$$\frac{\Delta\mathrm{T_L}}{\mathrm{T}} = \frac{2\mathrm{Re}\left(E_{\mathrm{o}}^{\mathrm{L}}(E_{\mathrm{s}}^{\mathrm{L}})^*\right)}{\left|E_{\mathrm{o}}^{\mathrm{L}}\right|^2} = \frac{(1+r)^2}{r}\left[\frac{\beta\chi_2(\cos2\theta-\sin2\theta)}{\sin2\theta} - \frac{\beta\chi_1}{\sin2\theta}\right]$$

$$\approx \frac{(1+r)^2}{r}\frac{\beta(\chi_2-\chi_1)}{\sin2\theta}. \quad (15)$$

$$\frac{\Delta\mathrm{T_R}}{\mathrm{T}} = \frac{2\mathrm{Re}\left(E_{\mathrm{o}}^{\mathrm{R}}(E_{\mathrm{s}}^{\mathrm{R}})^*\right)}{\left|E_{\mathrm{o}}^{\mathrm{R}}\right|^2} = \frac{(1+r)^2}{r}\left[\frac{\beta\chi_1}{\sin2\theta} + \frac{\beta\chi_2(\cos2\theta-\sin2\theta)}{\sin2\theta}\right]$$

$$\approx \frac{(1+r)^2}{r}\frac{\beta(\chi_2+\chi_1)}{\sin2\theta}. \quad (16)$$

Thus, we could see that the optical signal will be universally increased by $(1+r)^2/r$ from transmission to reflection configuration.

Supplementary Note 4. Estimate the sensitivity of our technique

This technique is based on the manipulation of interference between incident left- (right-) handed elliptically polarized light and materials' scattering light., physically this technique is not limited to CNTs, but establishes a general analytical means for the entire class of 1D materials. The only limitation should come from the signal-to-noise level of other 1D systems. Here we consider the detection limit of our technique and estimate how far our technique can go for other 1D materials with possible smaller signal. Firstly, according to the performance of our detector (linear CCD, Imaging Solution Group, LW ELIS-1024a-1394, 14 bit), the minimum contrast signal that can be measured is about 10^{-4} (the average of sufficient data to minimize the random noise is needed). Secondly, considering ~20-100 times enhancement of the technique based on polarization manipulation, the detection limit of our technique could be ~10^{-6}.

Supplementary References:

1. Liu, K., Deslippe, J., Xiao, F., Capaz, R.B., Hong, X. et al. An atlas of carbon nanotube optical transitions. *Nat Nanotechnol* **7**, 325-329 (2012).
2. Liu, K.H., Hong, X.P., Choi, S., Jin, C.H., Capaz, R.B. et al. Systematic determination of absolute absorption cross-section of individual carbon nanotubes. *PNAS* **111**, 7564-7569 (2014).
3. Lindfors, K., Kalkbrenner, T., Stoller, P. & Sandoghdar, V. Detection and spectroscopy of gold nanoparticles using supercontinuum white light confocal microscopy. *Phys Rev Lett* **93**, 037401 (2004).
4. Heinz, T.F. Rayleigh scatteing spectroscopy. *Carbon Nanotubes* **111**, 353-369 (Springer, 2007).
5. Malic, E., Hirtschulz, M., Milde, F., Wu, Y., Maultzsch, J. et al. Theory of Rayleigh scattering from metallic carbon nanotubes. *Phys Rev B* **77**, 045432 (2008).